Journal of Thermal Analysis and Calorimetry (2020) 140:789–797
https://doi.org/10.1007/s10973-019-08933-y

# Entropy generation in peristalsis with iron oxide

Bilal Ahmed[1] · T. Hayat[1,2] · A. Alsaedi[2] · F. M. Abbasi[3]

Received: 23 April 2019 / Accepted: 18 October 2019 / Published online: 31 October 2019


## Abstract

Entropy generation in peristaltic transport of nanomaterial with iron oxide is discussed. MHD and Joule heating are analyzed. Energy equation further consists of heat source/sink and viscous dissipation. Velocity slip and temperature jump conditions are also accounted. Large wavelength analysis is carried out. Results for velocity, temperature, pressure and entropy generation are presented graphically. Temperature decreases by increasing nanomaterials' volume fraction. Larger velocity slip parameter yields lower pressure gradient. Entropy generation is increased for Hartmann number and nanoparticle volume fraction.

**Keywords** Peristalsis · Iron oxide · Hartmann number · Slip effects · Entropy generation

## Introduction

Nanofluid constitutes of suspension of nanometer-sized particles in ordinary fluid. In the modern industry, biotechnology and pharmacological processes, distinct types of nanoparticles are used. Nanoparticles having unique physical properties due to their large surface area have dominating role by small bulk of material. Applications of nanoparticles in biological systems include omic data generation, bioimaging, cell tracking, artificial organ generation, tissue engineering, cancer therapy, biosensors, drug delivery, subcellular fractionation and nanoscopy. Molecular imaging of cells and tissues using nanotechnology technique creates opportunities for noninvasive diagnosis of various diseases including cancer [1, 2]. Firstly, Choi [3] explored the unique features of nanosized particles. Buongiorno gave theoretical model [4] to solve the nanofluid problems. Brownian diffusion and thermophoresis parameters are introduced for nanofluid description. Tiwari and Das also gave another model to study the viscous nanofluid [5]. Preference of this model is that we use the specific values verified by experiments for thermal conductivity, viscosity, specific heat and electrical conductivity of nanoparticles and base fluid. There are different models for thermal conductivity of nanofluid in the literature [6]. Maxwell, Hamilton–Crosser and Xue models are most accurate for describing the characteristics of thermal conductivity [7–9]. According to these models, the thermal conductivity of particle suspension compared to their ordinary fluid is enhanced. Numerous factors affecting thermal conductivity of nanofluid are described. Three important factors are nanoparticle size, material and temperature. Hayat et al. [10] investigated distinct types and size of nanoparticles and additional temperature effects. Effective viscosity of nanofluid is enhanced by decaying temperature and increasing nanomaterials volume fraction. Some valuable related works [11–23] have been published covering different aspects of nanofluid.

Peristalsis has important role in various biological and industrial processes. Here, contraction and expansion of the vessels wall generate the fluid motion [24]. Physiological processes in this direction may include chyme movement through intestine, blood flow through arteries and intrauterine fluid flow via uterus, etc. The uterus in women of reproductive age presents an intrinsic contraction and expansion within the sub-endometrial myometrium known as uterine peristalsis. It changes periodically. Their direction and frequency depend on the menstrual cycle phase. Uterine peristalsis preforms a vital role in such functions as

✉ Bilal Ahmed
bilalqau01@gmail.com

1 Department of Mathematics, Quaid-I-Azam University, 45320, Islamabad 44000, Pakistan

2 Nonlinear Analysis and Applied Mathematics (NAAM) Research Group, Faculty of Science, King Abdulaziz University, 80203, Jeddah 21589, Saudi Arabia

3 Department of Mathematics, COMSATS University Islamabad, Islamabad 44000, Pakistan

menstrual blood discharge, sperm transport and preservation of pregnancies during the initial stages of pregnancy [25]. Engineering applications of peristaltic flows are found in dialysis machines, heat lung, hose pumps, finger and roller pumps. Studies examining the mechanism of peristaltic transport can be seen through Refs. [26–28]. Peristaltic flow of nanofluid is significant in the modern drug delivery procedures. Hayat et al. [29] explored convective peristaltic flow of Carreau–Yasuda nanofluid in the presence of magnetic field. In modern technology, magneto-nanofluids gain much more attention due to its valuable use in industry and biomedical sciences. Such motivation is due to the application of magnetic field in hyperthermia, reduction in bleeding during surgery, removal of blockage in the arteries, cancer tumor, polymer technology, electrostatic precipitation, in molten metals purification from nonmetallic inclusion and MHD generation. Abbasi et al. [30] explored peristaltic motion of nanofluid for the drug delivery systems. Hayat et al. [31] numerically investigated the peristaltic motion of magneto-nanofluid in the presence of modified Darcy law. Liang et al. [32] examined velocity slip on shear stress in membrane system. The wall slip is significant for describing the macroscopic effects of certain molecular phenomena in the study of fluid–solid interaction problems. The significant application of slip effect in modern technology is polishing of artificial heart. Abbas et al. [33] explained the nanofluid motion in circular cylinder with velocity and thermal slips.

Entropy generation demonstrates the location of a system in which more energy dissipation occurs. Bejan [34] studied the prime factor to modify the entropy generation phenomenon. Since entropy is one factor out of numerous for the wastage of energy through heat transfer process, it becomes essential to measure entropy generation in a more precise manner. Addition of nanomaterials in a base fluid improves the heat transfer efficiency of liquids. However, it also enhances the viscosity of fluid and therefore fluid flow pressure loss. Furthermore, improvement in heat transfer characteristics effectively reduces entropy generation and irreversibility. Manay et al. [35] examined the entropy generation of nanofluid in a microchannel. Khan et al. [36] explored entropy generation minimization of nanofluid. Further, they have studied the nonlinear thermal radiation. Noreen et al. [37] studied entropy generation analysis in a tube with viscous dissipation. Prime purpose of this study is to explore entropy generation in peristaltic transport of nanofluid with combined effects of MHD, Ohmic heating and viscous dissipation. Further, velocity slip and thermal jump conditions are considered. Numerical simulation is used for describing the velocity, temperature, pressure gradient and entropy generation. Physical interpretation of obtained results is explored through graphs. The proposed mathematical model has relevance with modern drug delivery processes and cancer therapy.

## Formulation

Peristaltic motion of nanofluid in a tube of radius $a$ is analyzed. Waves in the speed c and wavelength $\lambda$ travel along the tube walls. We select a cylindrical coordinates system $(\bar{R}, \bar{Z})$. Here, $\bar{Z}$-axis lies along the centerline and $R$-axis in radial direction. Wall surface is described by [37]:

$$\bar{h} = a + b\sin\frac{2\pi}{\lambda}(\bar{Z} - c\bar{t}), \tag{1}$$

where $b$ indicates wave amplitude and $t$ time. Nanofluid is mixture of nanoparticles and ordinary fluid. Water is considered as an ordinary fluid and iron oxide nanosized particles as nanomaterials. These are considered to be in thermal equilibrium. For the present problem, Brinkman viscosity model is considered for $\mu_{\rm nf}$ as [13]:

$$\mu_{\rm nf} = \frac{\mu_{\rm w}}{(1-\phi)^{2.5}}, \tag{2}$$

where $\mu_{\rm w}$ denotes viscosity of conventional liquid and $\phi$ depicts nanomaterials volume fraction. In view of Maxwell model, the effective thermal conductivity of nanofluid is [7]:

$$\frac{K_{\rm nf}}{K_{\rm w}} = \frac{K_{\rm np} + 2K_{\rm w} - 2\varphi(K_{\rm w} - K_{\rm np})}{K_{\rm np} + 2K_{\rm w} + \varphi(K_{\rm w} - K_{\rm np})}. \tag{3}$$

The density of nanoliquids $\rho_{\rm nf}$, heat capacity of nanoliquid $(\rho C)_{\rm nf}$, thermal expansion of nanoliquid $(\rho\beta)_{\rm nf}$ and electric conductivity $(\sigma_{\rm nf})$ are given as follows [10]:

$$\rho_{\rm nf} = (1-\phi)\rho_{\rm w} + \phi\rho_{\rm np},\ (\rho C)_{\rm nf} = (1-\phi)(\rho C)_{\rm w} + \phi(\rho C)_{\rm np},$$
$$(\rho\beta)_{\rm nf} = (1-\phi)(\rho\beta)_{\rm w} + \phi(\rho\beta)_{\rm np},\ \frac{\sigma_{\rm nf}}{\sigma_{\rm f}} = 1 + \frac{3\left(\frac{\sigma_{\rm np}}{\sigma_{\rm w}}-1\right)\phi}{\left(\frac{\sigma_{\rm np}}{\sigma_{\rm w}}+2\right)-\left(\frac{\sigma_{\rm np}}{\sigma_{\rm w}}-1\right)\phi}. \tag{4}$$

Magnetic field of constant strength $B_0$ is applied. Induced magnetic field for small magnetic Reynolds number is neglected. The wave $(\bar{r}, \bar{z})$ and laboratory $(\bar{R}, \bar{Z}, \bar{t})$ are related by [10]:

$$\bar{r} = \bar{R},\ \bar{z} = \bar{Z} - c\bar{t},\ \bar{u} = \bar{U},\ \bar{w} = \bar{W} - c,\ \bar{p}(\bar{z}, \bar{r}) = \bar{P}(\bar{Z}, \bar{R}, \bar{t}). \tag{5}$$

Here, $(\bar{U}, \bar{W})$ and $\bar{P}$ denote the velocity components and pressure in the laboratory frame $(\bar{Z}, \bar{R}, \bar{t})$, and $(\bar{u}, \bar{w})$ and $\bar{p}$ represent the velocities and pressure in the wave frame $(\bar{z}, \bar{r})$ of reference. The governing mathematical expression in the wave frame is given by [10, 37]:

$$\frac{1}{r}\frac{\partial(\bar{r}\bar{u})}{\partial\bar{r}}+\frac{\partial\bar{w}}{\partial\bar{z}}=0, \tag{6}$$

$$\rho_{\mathrm{nf}}\left(\bar{u}\frac{\partial}{\partial\bar{r}}+(\bar{w}+c)\frac{\partial}{\partial\bar{z}}\right)\bar{u}=-\frac{\partial\bar{p}}{\partial\bar{r}}+\mu_{\mathrm{nf}}\left(2\frac{\partial^2\bar{u}}{\partial\bar{r}^2}+\frac{2}{r}\frac{\partial\bar{u}}{\partial\bar{r}}-2\frac{\bar{u}}{\bar{r}^2}\right)+\mu_{\mathrm{nf}}\frac{\partial}{\partial\bar{z}}\left[\frac{\partial\bar{u}}{\partial\bar{r}}+\frac{\partial\bar{w}}{\partial\bar{z}}\right], \tag{7}$$

$$\rho_{\mathrm{nf}}\left(\bar{u}\frac{\partial}{\partial\bar{r}}+(\bar{w}+c)\frac{\partial}{\partial\bar{z}}\right)(\bar{w}+c)=-\frac{\partial\bar{p}}{\partial\bar{z}}+\mu_{\mathrm{nf}}\left[\frac{\partial}{\partial\bar{z}}\left(2\frac{\partial\bar{w}}{\partial\bar{z}}\right)+\frac{1}{r}\frac{\partial}{\partial\bar{r}}\left(r\left(\frac{\partial\bar{u}}{\partial\bar{z}}+\frac{\partial\bar{w}}{\partial\bar{r}}\right)\right)\right]-\sigma_{\mathrm{nf}}B_0^2(\bar{w}+c), \tag{8}$$

$$(\rho C)_{\mathrm{nf}}\left(\bar{u}\frac{\partial T}{\partial\bar{r}}+(\bar{w}+c)\frac{\partial T}{\partial\bar{z}}\right)=K_{\mathrm{nf}}\left(\frac{\partial^2T}{\partial\bar{r}^2}+\frac{1}{r}\frac{\partial T}{\partial\bar{r}}+\frac{\partial^2T}{\partial\bar{z}^2}\right)+\sigma_{\mathrm{nf}}B_0^2(\bar{w}+c)^2+\mu_{\mathrm{nf}}\left[2\left(\left(\frac{\partial\bar{u}}{\partial\bar{r}}\right)^2+\left(\frac{\partial\bar{w}}{\partial\bar{z}}\right)^2\right)+\left(\frac{\partial\bar{u}}{\partial\bar{z}}+\frac{\partial\bar{w}}{\partial\bar{r}}\right)^2\right]+\boldsymbol{\Phi}, \tag{9}$$

where $\boldsymbol{\Phi}$ stands for dimensional heat absorption/generation. We consider the following dimensionless variables [10, 37]:

$$z=\frac{\bar{z}}{\lambda},\ r=\frac{\bar{r}}{a},\ w=\frac{\bar{w}}{c},\ u=\frac{\bar{u}}{c\delta},\ \delta=\frac{a}{\lambda},\ h=\frac{\bar{H}}{a},\ p=\frac{a^2\bar{p}}{c\lambda\mu_{\mathrm{w}}},\ \mathrm{Re}=\frac{\rho_{\mathrm{w}}\mathrm{ca}}{\mu_{\mathrm{w}}},\ \mathrm{Ec}=\frac{c^2}{C_{\mathrm{w}}T_0},\ \mathrm{Pr}=\frac{\mu_{\mathrm{w}}C_{\mathrm{w}}}{K_{\mathrm{w}}},\ \mathrm{M}=\sqrt{\frac{\sigma_{\mathrm{w}}}{\mu_{\mathrm{w}}}}B_0a,\ \theta=\frac{T-T_0}{T_0},\ \mathrm{Br}=\mathrm{Pr}\,\mathrm{Ec},\ \varepsilon=\frac{a^2\boldsymbol{\Phi}}{K_{\mathrm{w}}}, \tag{10}$$

where $\mathrm{Re},\ \mathrm{Br},\ \mathrm{Ec},\ \mathrm{Pr},\ \mathrm{M},\ \delta,\ \theta$ and $\varepsilon$ denote the Reynolds number, Brinkman parameter, Eckert number, Prandtl number, Hartmann number, wave number, nondimensional temperature and heat source/sink parameters, respectively. The assumption of long wavelength ($\delta \approx 0$) and small Reynolds number ($Re \approx 0$) is extensively used in the study of peristaltic motion. In view of the long wavelength and small Reynolds number assumptions, we have

$$\frac{\partial p}{\partial r}=0, \tag{11}$$

$$\frac{\partial p}{\partial z}=\frac{1}{(1-\varphi)^{2.5}}\frac{1}{r}\frac{\partial}{\partial r}\left(r\frac{\partial w}{\partial r}\right)-\frac{\sigma_{\mathrm{nf}}}{\sigma_{\mathrm{f}}}\mathrm{M}^2(w+1), \tag{12}$$

$$\frac{K_{\mathrm{nf}}}{K_{\mathrm{f}}}\frac{1}{r}\frac{\partial}{\partial r}\left(r\frac{\partial\theta}{\partial r}\right)+\frac{\mathrm{Br}}{(1-\varphi)^{2.5}}\left(\frac{\partial w}{\partial r}\right)^2+\frac{\sigma_{\mathrm{nf}}}{\sigma_{\mathrm{f}}}\mathrm{Br}\mathrm{M}^2(w+1)^2+\varepsilon=0. \tag{13}$$

Continuity equation is trivially justified, and Eq. (11) depicts that $p \neq p(r)$. The nondimensional form of flow rate in the fixed $\eta(=\bar{Q}/\mathrm{ca})$ and moving $F(=\bar{q}/\mathrm{ca})$ frames of reference is related by:

$$\eta=F+\frac{1}{2}\left(1+\frac{\zeta^2}{2}\right). \tag{14}$$

Here, $\bar{Q}$ and $\bar{q}$ are dimensional forms of flow rates in the fixed and moving frames. Furthermore, '$F$' is given as:

$$F=2\pi\int_0^h rw\,\mathrm{d}r. \tag{15}$$

The associated boundary conditions are [10]:

$$\frac{\partial w}{\partial r}=0,\ \frac{\partial\theta}{\partial r}=0,\ \text{at } r=0,\qquad w+\frac{\beta}{(1-\varphi)^{2.5}}\frac{\partial w}{\partial r}=-1,\ \theta+\gamma\frac{\partial\theta}{\partial r}=0,\ \text{at } r=h. \tag{16}$$

Here, $h=1+a\sin(2\pi x)$ depicts the nondimensional configuration of peristaltic wall, $\beta$ represents the dimensionless velocity slip parameter and $\gamma$ stands for dimensionless thermal slip parameter. Here, we use the Mathematica 9 software to compute the numerical solutions via NDSolve technique. This technique guarantees the accuracy in solution of the boundary value problem using suitable step size. In this problem, we have chosen step size 0.01 for the variation in both $x$ and $y$.

## Entropy generation analysis

Entropy generation expression can be defined as follows [37–40]:

$$S_{\mathrm{G}}=\frac{K_{\mathrm{nf}}}{\bar{T}_0^2}\left(\left(\frac{\partial T}{\partial\bar{r}}\right)^2+\left(\frac{\partial T}{\partial\bar{z}}\right)^2\right)+\frac{\sigma_{\mathrm{nf}}}{\bar{T}_0}B_0^2(\bar{w}+c)^2+\frac{\mu_{\mathrm{nf}}}{\bar{T}_0}\left[2\left(\left(\frac{\partial\bar{u}}{\partial\bar{r}}\right)^2+\left(\frac{\partial\bar{w}}{\partial\bar{z}}\right)^2\right)+\left(\frac{\partial\bar{u}}{\partial\bar{z}}+\frac{\partial\bar{w}}{\partial\bar{r}}\right)^2\right]. \tag{17}$$

$$N_{\mathrm{S}}=\frac{K_{\mathrm{nf}}}{K_{\mathrm{f}}}\left(\frac{\partial\theta}{\partial\bar{r}}\right)^2+\frac{\mathrm{Br}}{(1-\varphi)^{2.5}}\left(\frac{\partial w}{\partial r}\right)^2+\frac{\sigma_{\mathrm{nf}}}{\sigma_{\mathrm{f}}}\mathrm{Br}\mathrm{M}^2(w+1)^2. \tag{18}$$

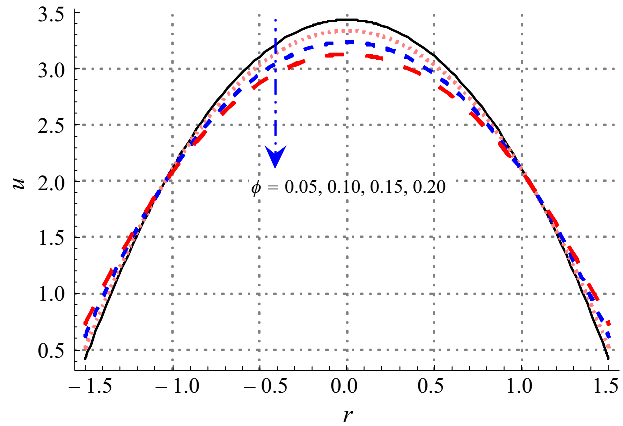


**Fig. 1** Effect of $\phi$ on velocity

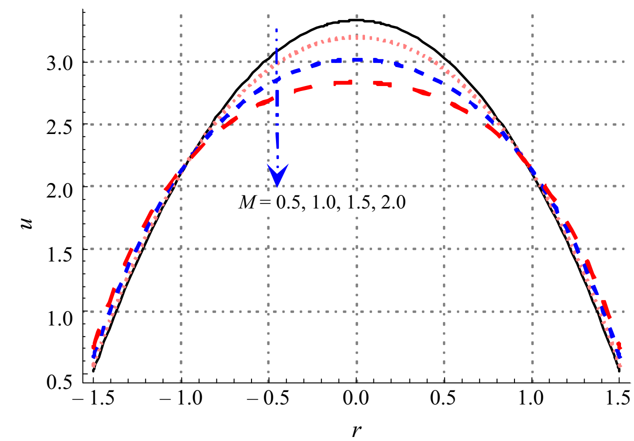


**Fig. 2** Effect of $M$ on velocity

**Table 1** Thermophysical characteristics [19]

| | $\rho$/kg m$^{-3}$ | $C_p$/J kg$^{-1}$K$^{-1}$ | $K$/W mk$^{-1}$ | $\beta$ (1/k)$\times 10^{-6}$ | $\sigma$/S m$^{-1}$ |
|---|---|---|---|---|---|
| $H_2O$ | 997.1 | 4179 | 0.613 | 210 | 0.05 |
| $Fe_3O_4$ | 5200 | 670 | 80.6 | 13 | 25,000 |

$N_S$ is the dimensionless form, and $S_G$ is known as entropy generation number. The total entropy generation can be written as

$$N_S = N_H + N_F + N_M, \tag{19}$$

where $N_H$ depicts the entropy generation effects caused by the presence of characteristic heat transfer, $N_F$ shows the entropy generation effect for the presence of fluid friction irreversibility and $N_M$ depicts the entropy generation effect for magnetic field. Bejan number (Be) gives the comparison between the total irreversibility and irreversibility due to heat transfer. Mathematically

$$\mathrm{Be} = \frac{N_H}{N_S}. \tag{20}$$

Clearly, Bejan number ranging from 0 to 1 holds when the entropy generation due to combined effects of fluid friction and magnetic field dominates. Bejan number approaching 1 is the opposite case where heat transfer irreversibility dominates and Bejan number of 0.5 corresponds to situation when contribution of both fluid friction and heat to entropy generation is equal.

## Discussion

Solutions of governing Eqs. (11)–(13) subject to boundary conditions (16) are determined. Graphical analysis of axial velocity, pressure gradient, pressure rise per wavelength, temperature and entropy is illustrated through Figs. 1–21. For graphical analysis, we have considered fixed numerical values of some parameters (Table 1).

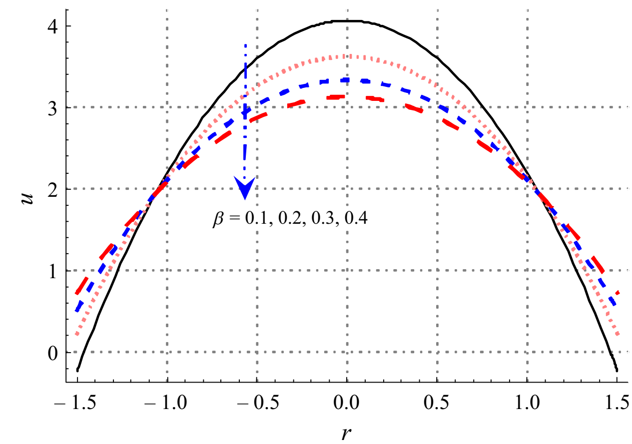


**Fig. 3** Effect of $\beta$ on velocity

## Velocity distribution

Figures 1–4 illustrate the analysis of axial velocity across the tube for nanomaterials volume fraction $\phi$, Hartmann number M, velocity slip parameter $\beta$ and amplitude ratio $\zeta$. Axial velocity reduces for larger value of nanomaterials volume fraction near center of tube (see Fig. 1). It is because of the fact that addition of nanomaterials provides more resistance to the flow and thus fluid velocity decays. Figure 2 indicates effects of Hartmann number on velocity distribution. It means that axial velocity reduces for larger applied magnetic field due to the retarding nature of Lorentz force. From Fig. 3, it is noted that axial velocity decreases near core part of tube by increasing velocity slip parameter and reverse behavior is seen near tube wall. It is noted from Fig. 4 that axial velocity decays by increasing the amplitude ratio.

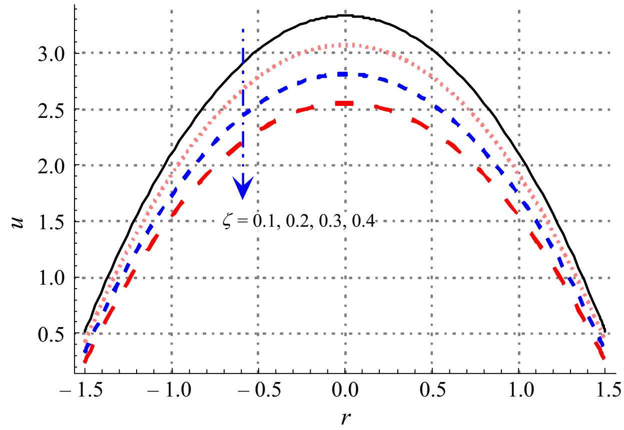


**Fig. 4** Effect of $\zeta$ on velocity

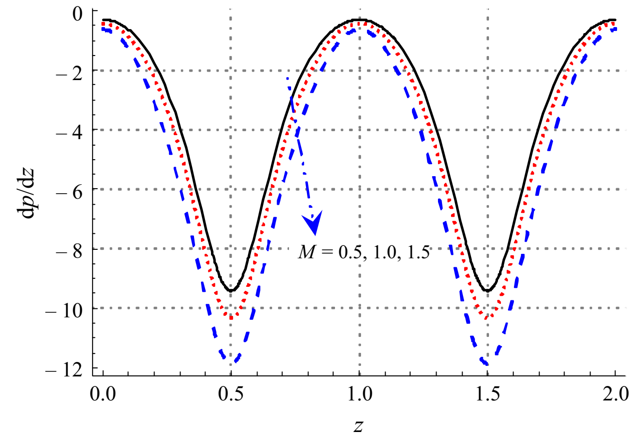


**Fig. 6** Effect of $M$ on $\mathrm{d}p/\mathrm{d}z$

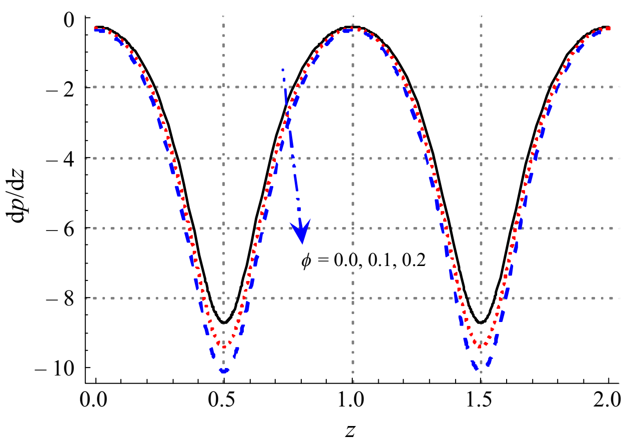


**Fig. 5** Effect of $\phi$ on $\mathrm{d}p/\mathrm{d}z$

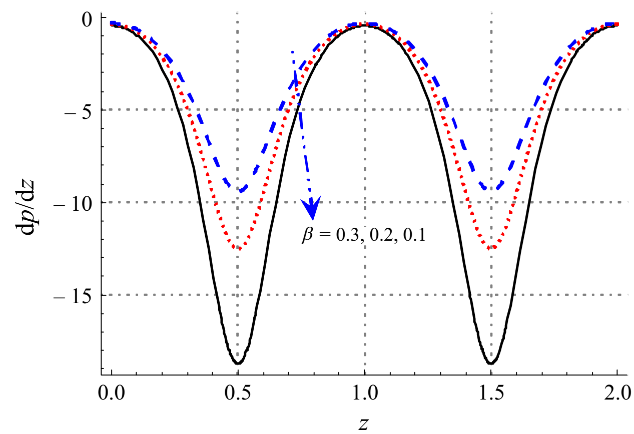


**Fig. 7** Effect of $\beta$ on $\mathrm{d}p/\mathrm{d}z$

## Pressure distribution

Figures 5–7 are plotted to examine the pressure gradient across the tube for various fluid parameters of interest. Figure 5 depicts that pressure gradient across the tube enhances larger nanomaterials volume fraction. It is due to the fact that resistance of fluid motion provided by the addition of nanomaterials is enhanced and therefore pressure gradient elevates. Figure 6 reveals that for large Hartmann number, the pressure gradient increases. Physically in the presence of strong magnetic field, more resistive force is experienced in system due to which more disturbances occurred and so pressure gradient is enhanced. Figure 7 studies influence of velocity slip on pressure gradient. It illustrates that an increase in $\beta$ decays pressure gradient in the tube and prominent effects are noticed in narrow portion. Figures 8–10 show study effects of

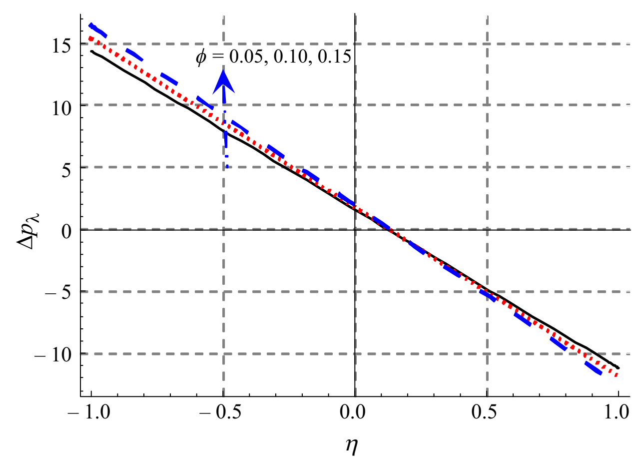


**Fig. 8** Effect of $\phi$ on $\Delta p_{\lambda}$

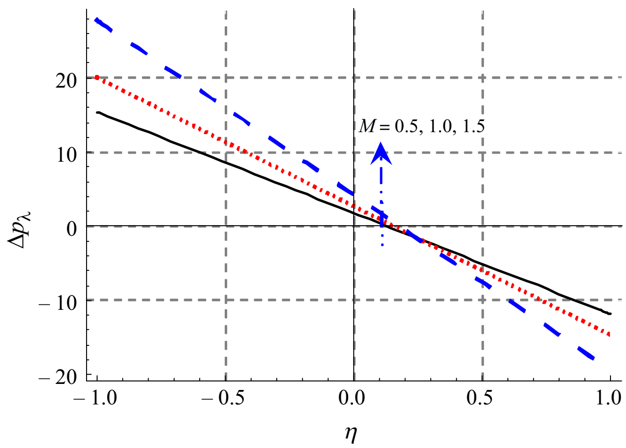


**Fig. 9** Effect of $M$ on $\Delta p_\lambda$

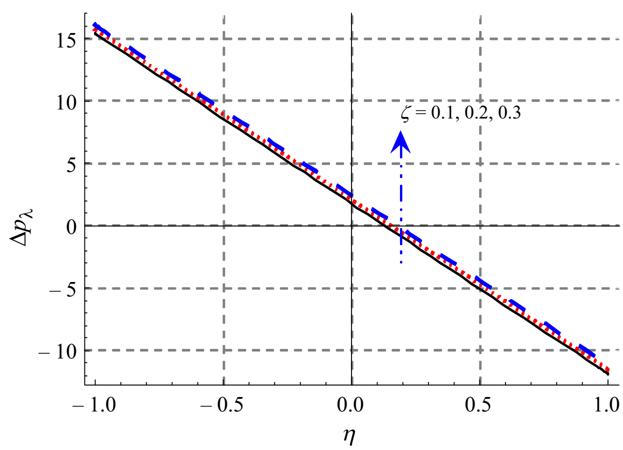


**Fig. 10** Effect of $\zeta$ on $\Delta p_\lambda$

pertinent variables on pressure rise per wavelength ($\nabla p_\lambda$). These graphs depict that when the flow rate is enhanced, then $\nabla p_\lambda$ decreases continuously. Graphs are generally classified in three regions known as retrograde, peristaltic and augmented pumping portions. Figures 8 and 9 show that by enhancing the nanoparticles volume fraction and Hartmann number, the pressure rise per wavelength decays in retrograde pumping region ($\eta < 0$, $\nabla p_\lambda > 0$) and peristaltic pumping region ($\eta < 0$, $\nabla p_\lambda < 0$). Furthermore, opposite trend is found in augmented pumping portion ($\eta > 0$, $\nabla p_\lambda < 0$). Figure 10 depicts that $\nabla p_\lambda$ increases by larger amplitude ratio parameter.

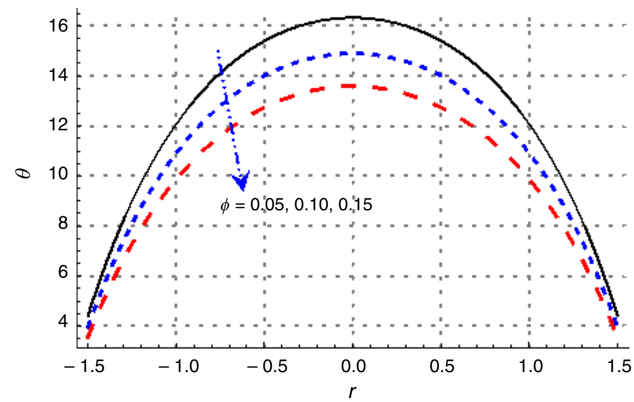


**Fig. 11** Effect of $\phi$ on temperature

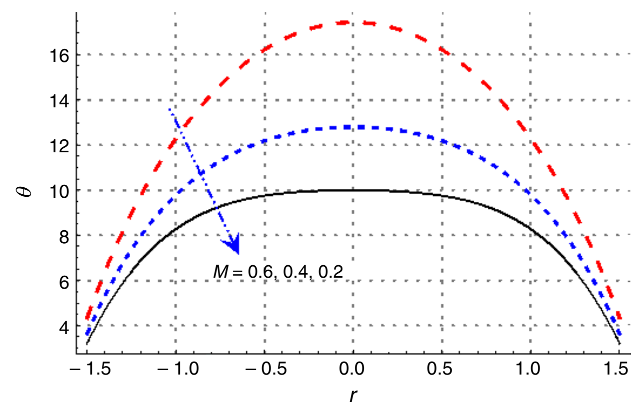


**Fig. 12** Effect of $M$ on temperature

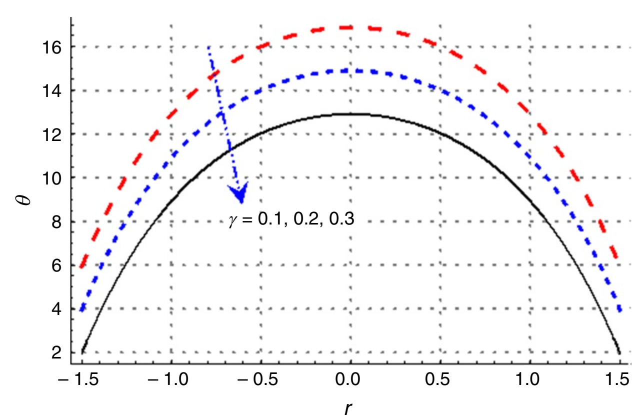


**Fig. 13** Effect of $\zeta$ on temperature

## Temperature distribution

Figures 11–13 display influences of $\phi$, M and $\gamma$ on temperature. Figure 11 indicates temperature for different nanomaterials volume fraction. Here, temperature rapidly decays for larger nanomaterials volume fraction. Nanoparticles play a role as cooling agent in fluid flow. Figure 12 gives effect of Hartmann number on temperature. Temperature is

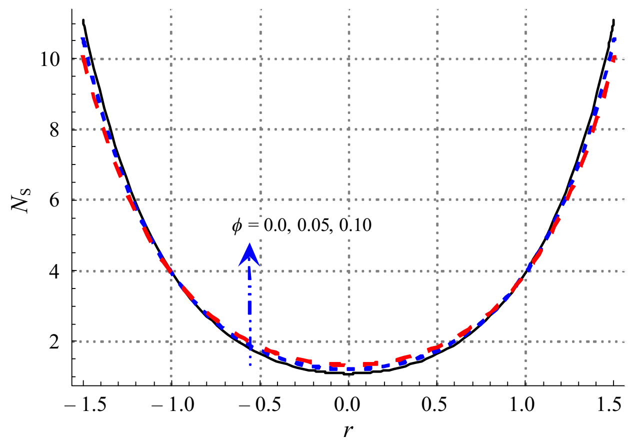


**Fig. 14** Effect of $\phi$ on $N_S$

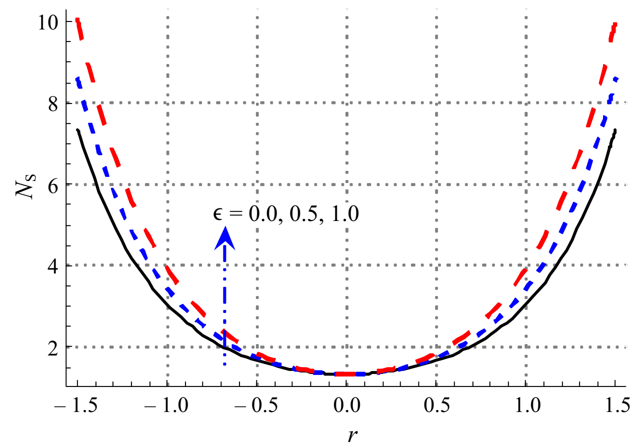


**Fig. 16** Effect of $\varepsilon$ on $N_S$

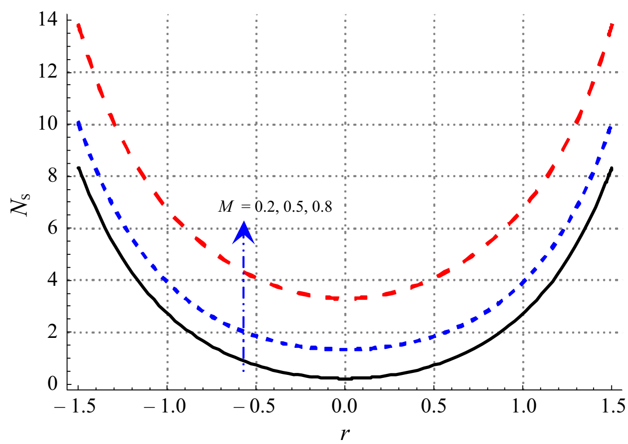


**Fig. 15** Effect of $M$ on $N_S$

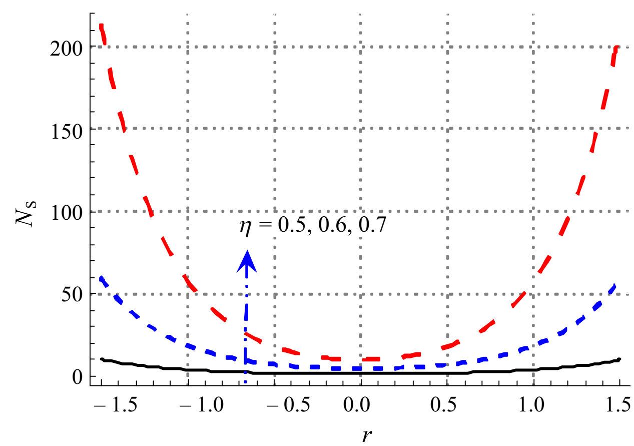


**Fig. 17** Effect of $\eta$ on $N_S$

enhanced for increasing the intensity of applied magnetic field due to Ohmic heating effect. Figure 13 illustrates that temperature uniformly decreases by increasing thermal jump parameter. Larger value of $\gamma$ parameter facilitates the heat transfer rate and therefore temperature decreases.

## Entropy distribution

Figures 14–17 are plotted to compute variations of $\phi$, M $\varepsilon$ and $\eta$ on entropy generation. Effect of nanomaterials volume fraction on entropy generation is observed in Fig. 14. It is examined that entropy generation is decreasing function of nanoparticle volume fraction. Figure 15 reveals that entropy generation enhances Hartmann number. Effect of heat source/sink on entropy generation is depicted in Fig. 16. Here, entropy generation is enhanced, especially near the tube wall for larger $\varepsilon$. Figure 17 depicts that there is a rise in entropy generation by flow rate parameter $\eta$. Effect of nanomaterials volume fraction on Bejan number is shown

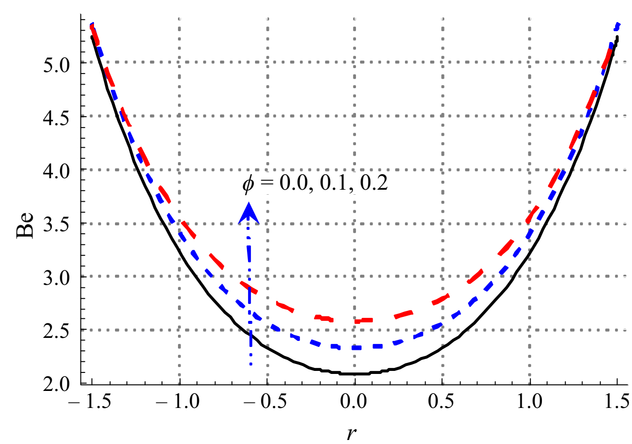


**Fig. 18** Effect of $\phi$ on Bejan number

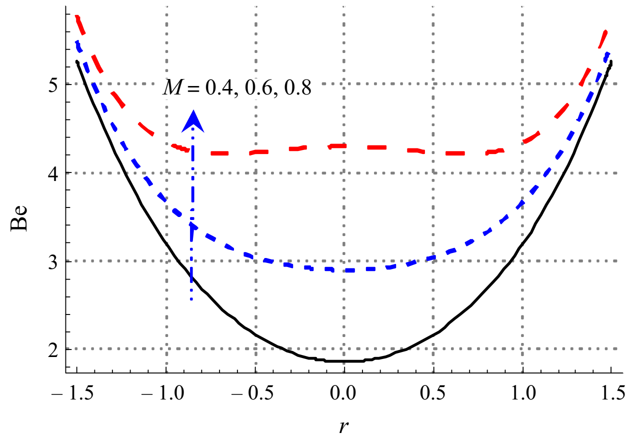


**Fig. 19** Effect of $M$ on Bejan number

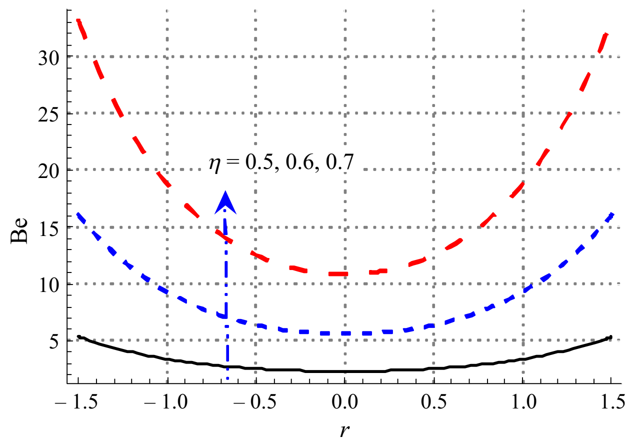


**Fig. 20** Effect of $\eta$ on Bejan number

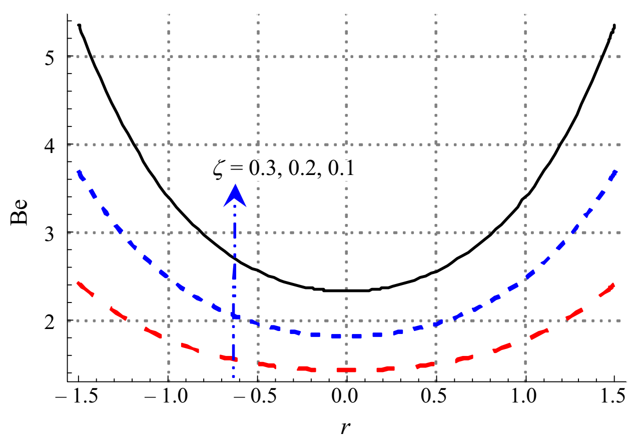


**Fig. 21** Effect of $\zeta$ on Bejan number

in Fig. 18. Bejan number is an increasing function of nanoparticle volume fraction. Figures 19 and 20 compute effects of Hartmann number and flow rate on Bejan number. It is noticed that Bejan number is enhanced via Hartmann number and flow rate. Figure 21 depicts that there is a reduction in Bejan number with increasing effect of amplitude ratio $\zeta$.

## Conclusions

Key points of this analysis are:

- Axial velocity shows decreasing behavior by increasing the nanoparticle volume fraction and Hartmann number.
- Presence of nanomaterials increases pressure gradient.
- Behavior of Hartmann number on pressure gradient is similar to nanomaterials volume fraction.
- Temperature decays via nanomaterial volume fraction.
- Temperature for Hartmann number has opposite response when compared with nanomaterial volume fraction.
- Presence of nanomaterials decreases entropy generation. Increasing the Hartmann number, the total entropy generation is remarkably enhanced.
- Bejan number has increasing behavior for nanoparticle volume fraction, Hartmann number and flow rate.

**Acknowledgements** We are grateful to Higher Education Commission (HEC) of Pakistan for financial support of this work under the Project No. 20-3088/NRPU/R&D/HEC/13.

## References

1. Dong S, Zheng L, Zhang X, Lin P. Improved drag force model and its application in simulating nanofluid flow. Microfluid Nanofluid. 2014;17:253–61.
2. Chamkha AJ, Molana M, Rahnama A, Ghadami F. On the nanofluids applications in microchannels: a comprehensive review. Powder Technol. 2018;332:287–322.
3. Choi SUS. Enhancing thermal conductivity of fluids with nanoparticles. ASME Fluids Eng Div. 1995;231:99–105.
4. Buongiorno J. Convective transport in nanofluids. J. Heat Transf. 2006;128:240–50.
5. Tiwari RJ, Das MK. Heat transfer augmentation in a two-sided lid-driven differentially heated square cavity utilizing nanofluids. Int J Heat Mass Transf. 2007;50:2002–18.
6. Alawi OA, Sidik NAC, Xian HW, Kean TH, Kazi SN. Thermal conductivity and viscosity models of metallic oxides nanofluids. Int J Heat Mass Transf. 2018;116:1314–25.
7. Maxwell JC. A treatise on electricity and magnetism. 2nd ed. Cambridge: Oxford University Press; 1904. p. 435–41.
8. Hamilton RL, Crosser OK. Thermal conductivity of heterogeneous two component systems. Ind Eng Chem Fundam. 1962;1:187–91.
9. Xue QZ. Model for thermal conductivity of carbon nanotube-based composites. Physica B Condens Matter. 2005;368:302–7.

10. Hayat T, Ahmed B, Abbasi FM, Alsaedi A. Hydromagnetic peristalsis of water based nanofluids with temperature dependent viscosity: a comparative study. J Mol Liq. 2017;234:324–9.
11. Khan LA, Raza M, Mir NA, Ellahi R. Effects of different shapes of nanoparticles in peristaltic flow of MHD nanofluids filled in an asymmetric channel: a novel mode for heat transfer enhancement. J Therm Anal Calorim. 2019. https://doi.org/10.1007/s10973-019-08348-9.
12. Nasiri H, Jamalabadi MYA, Sadeghi R, Safaei MR, Nguyen TK, Shadloo MS. A smoothed particle hydrodynamics approach for numerical simulation of nano-fluid flows. J Therm Anal Calorim. 2019;135:1733–41.
13. Brickman HC. The viscosity of concentrated suspensions and solutions. J Chem Phys. 1952;20:571–81.
14. Bhatti MM, Zeeshan A, Ellahi R, Bég OA, Kadir A. Effects of coagulation on the two phase peristaltic pumping of magnetized Prandtl biofluid through an endoscopic annular geometry containing a porous medium. Chin J Phys. 2019;58:222–34.
15. Ellahi R, Hassan M, Zeeshan A. Shape effects of nanosize particles in Cu–$H_2O$ nanofluid on entropy generation. Int J Heat Mass Transf. 2015;81:449–56.
16. Sheikholeslami M, Hayat T, Alsaedi A. On simulation of nanofluid radiation and natural convection in an enclosure with elliptical cylinders. Int J Heat Mass Transf. 2017;115:981–91.
17. Ul Haq R, Nadeem S, Khan ZH, Noor NFM. MHD squeezed flow of water functionalized metallic nanoparticles over a sensor surface. Physica E Low-Dimens Syst Nanostruct. 2015;73:45–53.
18. Hayat T, Muhammad K, Alsaedi A. Melting effect in MHD stagnation point flow of Jeffrey nanomaterial. Physica Scripta. 2019;94:115702. https://iopscience.iop.org/article/10.1088/1402-4896/ab210e/meta.
19. Ellahi R, Zeeshan A, Hussain F, Asadollahi A. Peristaltic blood flow of couple stress fluid suspended with nanoparticles under the influence of chemical reaction and activation energy. Symmetry. 2019;11:276.
20. Hayat T, Aziz A, Muhammad T, Alsaedi A. Numerical simulation for Darcy–Forchheimer three-dimensional rotating flow of nanofluid with prescribed heat and mass flux conditions. J Therm Anal Calorim. 2019;136:2087–95.
21. Khan AA, Masood F, Ellahi R, Bhatti MM. Mass transport on chemicalized fourth-grade fluid propagating peristaltically through a curved channel with magnetic effects. J Mol Liq. 2018;258:186–95.
22. Hayat T, Muhammad K, Alsaedi A, Asghar S. Numerical study for melting heat transfer and homogeneous–heterogeneous reactions in flow involving carbon nanotubes. Results Phys. 2018;8:415–21.
23. Hayat T, Aziz A, Muhammad T, Alsaedi A. Significance of homogeneous–heterogeneous reactions in Darcy–Forchheimer three-dimensional rotating flow of carbon nanotubes. J Therm Anal Calorim. 2019. https://doi.org/10.1007/s10973-019-08316-3.
24. Hayat T, Abbasi FM, Ahmed B. Peristaltic transport of copper–water nanofluid saturating porous medium. Physica E. 2015;67:47–53.
25. Liu S, Zhang Q, Yin C, Chen W, Chan Q, He J, Zhu B. An optimised repetition time (TR) for cine imaging of uterine peristalsis on 3 T MRI. Clin Radiol. 2018;73:7–12.
26. Hayat T, Ahmed B, Abbasi FM, Alsaedi A. Flow of carbon nanotubes submerged in water through a channel with wavy walls with convective boundary conditions. Colloid Polym Sci. 2017;295:1905–14.
27. Ali N, Sajid M, Javed T, Abbas Z. Heat transfer analysis of peristaltic flow in a curved channel. Int J Heat Mass Transf. 2017;53:3319–25.
28. Hayat T, Ahmed B, Abbasi FM, Ahmad B. Mixed convective peristaltic flow of carbon nanotubes submerged in water using different thermal conductivity models. Comput Methods Programs Biomed. 2016;135:141–50.
29. Hayat T, Ahmed B, Alsaedi A, Abbasi FM. Numerical study for peristalsis of Carreau–Yasuda nanomaterial with convective and zero mass flux condition. Results Phys. 2018;8:1168–77.
30. Abbasi FM, Hayat T, Ahmad B. Peristalsis of silver–water nanofluid in the presence of Hall and Ohmic heating effects: applications in drug delivery. J Mol Liq. 2015;207:248–55.
31. Hayat T, Ahmed B, Abbasi FM, Alsaedi A. Numerical investigation for peristaltic flow of Carreau–Yasuda magneto-nanofluid with modified Darcy and radiation. J Therm Anal Calorim. 2019;137:1359–67.
32. Liang YY, Weihs GAF, Fletcher DF. CFD study of the effect of unsteady slip velocity waveform on shear stress in membrane systems. Chem Eng Sci. 2018;192:16–24.
33. Abbas N, Saleem S, Nadeem S, Alderremy AA, Khan AU. On stagnation point flow of a micro polar nanofluid past a circular cylinder with velocity and thermal slip. Results Phys. 2018;9:1224–32.
34. Bejan A. Entropy generation minimization. Boca Raton: CRC Press; 1996.
35. Manay E, Akyürek EF, Sahin B. Entropy generation of nanofluid flow in a microchannel heat sink. Results Phys. 2018;9:615–24.
36. Khan MWA, Khan MI, Hayat T, Alsaedi A. Entropy generation minimization (EGM) of nanofluid flow by a thin moving needle with nonlinear thermal radiation. Physica B Condens Matter. 2018;534:113–9.
37. Akbar NS, Butt AW. Entropy generation analysis for the peristaltic flow of Cu–water nanofluid in a tube with viscous dissipation. J Hydrodyn. 2017;29:135–43.
38. Abbasi FM, Shanakhat I, Shehzad SA. Entropy generation analysis for peristalsis of nanofluid with temperature dependent viscosity and Hall effects. J Magn Magn Mater. 2019;474:434–41.
39. Zeeshan A, Shehzad N, Abbas T, Ellahi R. Effects of radiative electro-magnetohydrodynamics diminishing internal energy of pressure-driven flow of titanium dioxide–water nanofluid due to entropy generation. Entropy. 2019;236:1–25.
40. Ijaz Khan M, Qayyum S, Hayat T, Imran Khan M, Alsaedi A. Entropy optimization in flow of Williamson nanofluid in the presence of chemical reaction and Joule heating. Int J Heat Mass Transf. 2019;133:959–67.


**Publisher's Note** Springer Nature remains neutral with regard to jurisdictional claims in published maps and institutional affiliations.